ICAS 2021 SHANGHAI
International Council of the Aeronautical Sciences
32nd Congress of the International Council of the Aeronautical Sciences
September 6-10, 2021
Pudong Shangri-La, Shanghai, China

ACCURATE MODELS FOR THE PREDICTION OF FREE-EDGE STRESSES OF COMPOSITE STRUCTURES UNDER THERMAL LOADS

E. Zappino[1] & E. Carrera[1]

[1]Mul2 group Department of Mechanical and Aerospace Engineering Politecnico di Torino Torino, Italy.

Abstract

The present paper presents a refined kinematic model for the prediction of the free-edge stress in composite structures under thermal loads. An advanced numerical model has been developed in the frameworks of the Carrera Unified Formulation, which allows any order structural theories to be considered. Equivalent single layer models, as well as, layer-wise formulations have been considered and compared. A node-dependent kinematic approach has been used to increase locally the accuracy of the solution. A coupled thermo-elastic formulation has been considered in order to consider general thermal loads. The model has been used to investigate the stresses at the free-edge of composite plates. Open literature results have been use to assess the present approach. The results show that the present model is able to predict the transverse stress concentrations that can originate delaminations and failures. The use of refined kinematic elements leads to a three-dimensional solution avoiding the huge computational costs of classical solid models

Keywords: free-edge, thermal loads, composite material, global-local, Carrera Unified Formulation.

1. Introduction

The development of the new generation of commercial aircraft has led to a large use of composite materials since they can ensure an high mechanical strength with a reduction of the overall weight of the structure. The design of composite structures, and in particular the prediction of their failure [12, 11, 13], has been the object of a massive number of numerical and experimental studies in the last decades but complex phenomena that can appear in such structures cannot always be investigated with the structural models used up to now.

The prediction of the limit loads for laminate structures requires an accurate analysis of the local stress field. The transverse stresses, usually neglected by the models used in the design of thin metallic structures, play a fundamental role in the delamination process that is, enhanced numerical approaches must be used [8]. Severe concentrations of transverse stresses may appear at the free-edge of laminates due to the different stiffness orientations of each layer. This phenomenon, named free-edge effect, has been the object of many studies and most of them propose to use a local refinement of the model to catch the stress concentration [6]. This phenomenon can be even more dangerous when the composite structure is subject to thermal loads [9] that may create a local stress field due to the orthotropy of the thermal expansion coefficients, an example is shown in Figure 1.

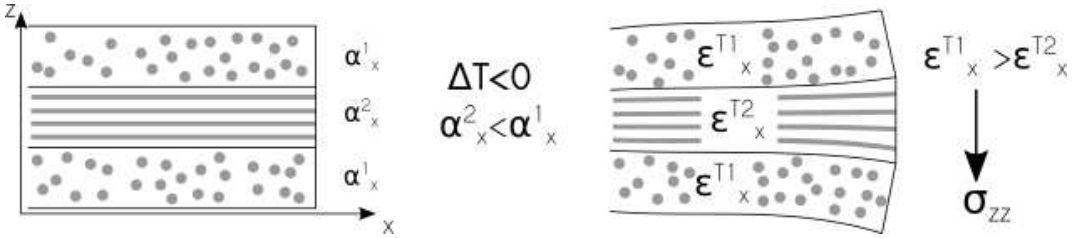

Figure 1 – Origin of the free-edge transverse stress due to thermal loads.

The aim of the present work is to exploit the enhanced capabilities of the models derived in the frameworks of the Carrera Unified Formulation, CUF,[3] to predict local free-edge effects of general laminate structures under thermal loads. The use of refined kinematic models allows a layer-wise description of the kinematic to be obtained; this capability makes it possible to predict with high accuracy the traversal and inter-laminar stresses [7]. The use of recent developments of the CUF, such those present in [5, 15], may increase the efficiency of the current approach refining the model locally, with huge advantages from the computational costs point of view. The capabilities of the present models to deal with multi-field problems, as demonstrated in [4], can be used to investigate complex load scenarios such as those due to complex thermal fields. The results show that the present approach can lead to a 3D-like solution with a significant reduction of the computational costs since two-dimensional model are adopted.

1.1 Preliminaries

This section presents the refined two-dimensional model used in the following analyses. The coordinate reference frame is shown in Fig. 2.

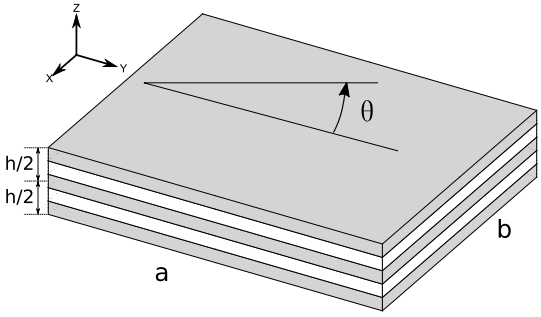

Figure 2 – Notation of a plate model for laminated structures.

The displacement three-dimensional field is described using the vector u:

$$u^T = \{u_x,\ u_y,\ u_z\} \tag{1}$$

In the thermo-elastic formulation, in addition to the mechanical variables, also the temperature variation, ϑ, must be considered. The solution of the thermo-elastic problem requires to define five quantities in each point:

$$q^T = \{u_x,\ u_y,\ u_z,\ \vartheta\} \tag{2}$$

where vector q contains the unknown quantities.

1.2 Geometrical relations

The geometrical relations in the case of the thermo-elastic model allow the strain (ε) and the thermal gradient (θ) to be evaluated. The strain vector, ε, can be written as:

$$\boldsymbol{\varepsilon}^T = \{\varepsilon_{xx}\ \varepsilon_{yy}\ \varepsilon_{zz}\ \varepsilon_{xz}\ \varepsilon_{yz}\ \varepsilon_{xy}\ \} = D_u u \tag{3}$$

where D_u is:

$$D_u^T = \begin{bmatrix} 0 & 0 & \partial_z & \partial_x & \partial_y & 0 \\ 0 & \partial_y & 0 & 0 & \partial_z & \partial_x \\ \partial_x & 0 & 0 & \partial_z & 0 & \partial_y \end{bmatrix} \tag{4}$$

The spatial temperature variation, θ, can be written as:

$$\boldsymbol{\theta}^T = \{\vartheta_x\ \vartheta_y\ \vartheta_z\} = D_\vartheta\, \vartheta \tag{5}$$

where D_ϑ is:

$$D_\vartheta^T = \begin{bmatrix} \partial_x & \partial_y & \partial_z \end{bmatrix} \tag{6}$$

1.3 Constitutive relations

The constitutive equation for the thermo-elastic model have been derived in according with the work presented by [1]. The stress, σ can be written in the following form:

$$\sigma = C\varepsilon - \lambda\vartheta \tag{7}$$

The first contribution come from the Hook's law and derives from the mechanical problem.

$$\begin{Bmatrix} \sigma_{xx} \\ \sigma_{yy} \\ \sigma_{zz} \\ \sigma_{xz} \\ \sigma_{yz} \\ \sigma_{xy} \end{Bmatrix} = \begin{bmatrix} C_{11} & C_{12} & C_{13} & 0 & 0 & C_{16} \\ C_{21} & C_{22} & C_{23} & 0 & 0 & C_{26} \\ C_{31} & C_{32} & C_{33} & 0 & 0 & C_{36} \\ 0 & 0 & 0 & C_{44} & C_{45} & 0 \\ 0 & 0 & 0 & C_{54} & C_{55} & 0 \\ C_{61} & C_{62} & C_{63} & 0 & 0 & C_{66} \end{bmatrix} \begin{Bmatrix} \varepsilon_{xx} \\ \varepsilon_{yy} \\ \varepsilon_{zz} \\ \varepsilon_{xz} \\ \varepsilon_{yz} \\ \varepsilon_{xy} \end{Bmatrix} \tag{8}$$

The second therm, $\lambda\vartheta$, comes from the thermo-mechanical coupling. The vector λ can be written as:

$$\lambda = C\alpha = C\{\alpha_1\ \alpha_2\ \alpha_3\ 0\ 0\ 0\ \}^T \tag{9}$$

Where C is the matrix with the elastic coefficients of the material, and α is the vector of the thermal expansion coefficients.
The last constitutive equation describe the heat flux, h:

$$h = \kappa\theta \tag{10}$$

where κ is the conductivity coefficients matrix:

$$\boldsymbol{\kappa} = \begin{bmatrix} \kappa_{11} & \kappa_{12} & 0 \\ \kappa_{21} & \kappa_{22} & 0 \\ 0 & 0 & \kappa_{33} \end{bmatrix} \tag{11}$$

1.4 Kinematic Model

This section introduced the kinematic assumption used in the present work. At first the CUF is presented. Models based on Equivalent single layer and layer-wise approaches are introduced and, finally the node-dependent kinematic model is introduced.

1.4.1 Carrera Unified Formulation (CUF) for refined 2D models

In the framework of CUF, the displacement field of a plate structure can be assumed to be:

$$\begin{aligned} u(x,y,z) &= F_0(z)u_0(x,y) \quad + F_1(z)u_1(x,y) \quad + \cdots + F_N(z)u_N(x,y) \\ v(x,y,z) &= F_0(z)v_0(x,y) \quad + F_1(z)v_1(x,y) \quad + \cdots + F_N(z)v_N(x,y) \\ w(x,y,z) &= F_0(z)w_0(x,y) \quad + F_1(z)w_1(x,y) \quad + \cdots + F_N(z)w_N(x,y) \end{aligned} \tag{12}$$

where the approximation functions $F_\tau(z)$ are also named as thickness functions. In a compact form, Equation 12 can be written as follows for ESL models:

$$\boldsymbol{u}(x,y,z) = F_\tau(z)\boldsymbol{u}_\tau(x,y) \qquad \tau = 0,1,...,N \tag{13}$$

in which $F_\tau(z)$ are defined on the domain through the whole thickness of the plate, which means $z \in [-\frac{h}{2}, \frac{h}{2}]$. Alternatively, for LW models, the displacements can be written as:

$$\boldsymbol{u}^k(x,y,\zeta_k) = F_\tau^k(\zeta_k)\boldsymbol{u}_\tau^k(x,y) \qquad \tau = 0,1,...,N \tag{14}$$

where k is the layer index, and $-1 \leq \zeta_k \leq 1$ is the adimensional thickness coordinate. The continuity conditions will be enforced at the layer interfaces.
$u_\tau^k(x,y)$ represent the unknown primary variables which are the factors corresponding to the expansion terms.

When the solution of the problem is achieved using the FE approach, equation 13 becomes:

$$\boldsymbol{u}(x,y,z) = F_\tau(z)N_i(x,y)u_{\tau i} \qquad \tau = 0,1,...,N, i = 0,1,...,M \tag{15}$$

Where the function N_i are the shape function used in the FE model. M is the number of nodes of each element.

1.5 ESL models based on Taylor expansions (TE)

In ESL models, Taylor series can be adopted as thickness functions by substituting $F_\tau = z^\tau (\tau = 0,1,\cdots,N)$ into Equation 13, and the obtained thickness functions of the higher-order model read:

$$F_0 = z^0 = 1, \quad F_1 = z^1 = z, \quad \ldots, \quad F_N = z^N \tag{16}$$

Especially, FSDT [10] can be obtained as a particular case of the complete linear model ($N = 1$).

1.6 LW models adopting Lagrange expansions (LE)

If F_τ^k are defined as Lagrange interpolation polynomials defined on layer k, as expressed in Equation 17, an LE-type LW model can be obtained. ζ_{k_τ} are located at the prescribed interpolation points. $\zeta_{k_0} = -1$ and $\zeta_{k_N} = 1$ in the natural reference system signifies the bottom and top surface of the kth layer, respectively.

$$F_\tau^k(\zeta_k) = \prod_{i=0, i\neq s}^{N} \frac{\zeta_k - \zeta_{k_i}}{\zeta_{k_\tau} - \zeta_{k_i}} \tag{17}$$

In LW models employing Lagrange expansions (LE), the displacements of each interpolation point are treated as unknown primary variables, and compatibility of the displacements at layer interfaces follows:

$$u_t^k = u_b^{k+1}, \quad k = 1,\cdots,N_l - 1. \tag{18}$$

in which N_l is the total number of layers. The continuity of transverse stresses at layer interfaces can be achieved when a sufficient number of expansion terms are used in each layer, as demonstrated in the authors' previous work [2].

1.7 A two-dimensional finite element with node-dependent kinematics

When the modeling of structural geometry or boundary conditions is beyond the capabilities of classical plate models, higher-order models can be used to improve the solution precision. In most cases, refined kinematics is necessary only in some local region of the whole structure, e.g. at the free edge, and classical models could be adequate elsewhere. A new class of node-dependent kinematic elements is introduced in this work to refine the kinematics only in the area necessary.

As an example, a four node two-dimensional element is considered. Refined plate elements with uniform kinematics assume the same thickness expansions in all the nodes. By using the node-dependent kinematic approach, a different kinematic assumption can be introduced at each node. The displacement field at the first node can be written as:

$$\boldsymbol{u}^1 = \boldsymbol{u}_{1\tau}F_\tau^1, \qquad \tau = 1\ldots M^1 \tag{19}$$

The displacement functions at the second node are:

$$\boldsymbol{u}^2 = \boldsymbol{u}_{2\tau}F_\tau^2, \qquad \tau = 1\ldots M^2 \tag{20}$$

The displacements at the third node read:

$$\boldsymbol{u}^3 = \boldsymbol{u}_{3\tau}F_\tau^3, \qquad \tau = 1\ldots M^3 \tag{21}$$

The displacements at the fourth node read:

$$\boldsymbol{u}^4 = \boldsymbol{u}_{4\tau}F_\tau^4, \qquad \tau = 1\ldots M^4 \tag{22}$$

The thickness expansions, F_τ^1, F_τ^2, F_τ^3 and F_τ^4, can be chosen arbitrarily at each node. At node 1, a first order TE model can be considered, and a LE model has been imposed at node 2 while a second order TE model is allocated to node 3 and 4. Eventually, the expression of the three-dimensional displacement field of the whole element becomes:

$$\boldsymbol{u} = \boldsymbol{u}_{1\tau} N_1 F_\tau^1 + \boldsymbol{u}_{2\tau} N_2 F_\tau^2 + \boldsymbol{u}_{3\tau} N_3 F_\tau^3 + \boldsymbol{u}_{4\tau} N_4 F_\tau^4, \qquad \tau = 1 \dots N^i \tag{23}$$

The four different displacement fields are smeared by the FE shape functions over the plate mid-plane. Using this approach, the continuity of the displacement is obtained at each point.
This approach can be easily included in the CUF formulation and extended to any order plate models. The displacement field of the two-dimensional element with node-dependent kinematic can be written including two main novelties:

$$F_\tau(z) \longrightarrow F_\tau^i(z) \tag{24}$$

$$N \longrightarrow N^i \tag{25}$$

The first equation, Eq. 24, states that the function expansion is not a property of the element, but of the nodes, that is, the index i is included in the notation. Eq. 25 remarks that the number of terms in the expansion, N, can be different at each node, and the notation N^i is used to underline this aspect. The generic displacement field can be written as:

$$\boldsymbol{u} = \boldsymbol{u}_{i\tau} N_i(y) F_\tau^i(x,z), \qquad \tau = 1 \dots N^i; \qquad i = 1 \dots N_n. \tag{26}$$

1.8 Governing equation

The governing equation can be written using the virtual displacements principle, PVD:

$$\delta L_{int} = \delta L_{ext} \tag{27}$$

where δL_{int} is the virtual variation of the internal work while, δL_{ext} is the virtual variation of the external work.
In explicit form the PVD can be written as:

$$\delta L_{int} = \int_V (\delta \varepsilon^T \sigma - \delta \theta^T h) dV = \delta L_{ext} \tag{28}$$

If geometrical and constitutive equation are substituted in Equation 28 the following equation is obtained:

$$\delta L_{int} = \int_V (\delta \varepsilon^T C \varepsilon - \delta \varepsilon^T \lambda \vartheta - \delta \theta^T \kappa \theta) dV \tag{29}$$

If the kinematic approximation introduced before is used the terms that compose the virtual variation of the internal work can be written in matrix form.
The first term, $\delta \varepsilon^T C \varepsilon$, represents the mechanical problem. The strain can be expressed in terms of derivatives of the displacements, moreover the displacements can be written using the shape functions N_i and F_τ.

$$\begin{aligned} \delta \varepsilon^T C \varepsilon =& \delta {q_u}_{js}^T \int_V N_j F_s^j I D_u^T C D_u I F_\tau^i N_i dV \, q_{ui\tau} = \\ =& \delta {q_u}_{js}^T k_{uu}^{ij\tau s} q_{ui\tau} \end{aligned} \tag{30}$$

$k_{uu}^{ij\tau s}$ is the fundamental nucleus of size 3×3 of the stiffness matrix of the pure mechanical problem. $q_{ui\tau}$ is the part of the unknown vector related to the mechanical variables.
The term $\delta \varepsilon^T \lambda \vartheta$ can be written as:

$$\begin{aligned} \delta \varepsilon^T \lambda \vartheta =& \delta {q_u}_{js}^T \int_V N_j F_s^j I D_u^T \lambda I F_\tau^i N_i dV \, q_{\vartheta i\tau} = \\ =& \delta {q_u}_{js}^T k_{u\theta}^{ij\tau s} q_{ui\tau} \end{aligned} \tag{31}$$

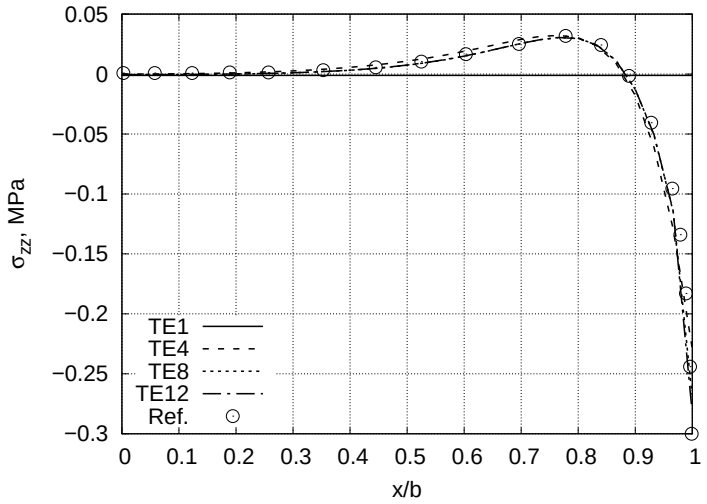

Figure 3 – σ_{zz} distribution evaluated using different equivalent single layer models, reference results from [14].

$k_{u\theta}^{ij\tau s}$ is the fundamental nucleus of size 3×1 of the stiffness matrix of the thermo-elastic problem. $q_{\vartheta i\tau}$ is the part of the unknown vector related to the thermal variable.
The term $\delta\theta^T\kappa\theta$ can be written as:

$$\begin{aligned}\delta\theta^T\kappa\theta =& \delta q_{\vartheta js}^T\int_V N_j F_s^j ID_\vartheta^T \kappa D_\vartheta IF_\tau^i N_i dV\, q_{\vartheta i\tau} = \\ =& \delta q_{u js}^T k_{\theta\theta}^{ij\tau s} q_{ui\tau}\end{aligned} \tag{32}$$

$k_{\theta\theta}^{ij\tau s}$ is the fundamental nucleus of size 1×1 of the stiffness matrix of the pure thermal problem.
All the fundamental nucleus can be assembled together in fundamental nucleus of the multi-field problem:

$$\delta L_{int} = \delta q_{js}^T \overbrace{\begin{bmatrix} \begin{bmatrix} \ddots & & \\ & k_{uu} & \\ & & \ddots \end{bmatrix} & \begin{bmatrix} \vdots \\ k_{u\theta} \\ \vdots \end{bmatrix} \\ \begin{bmatrix} \cdots & 0 & \cdots \end{bmatrix} & \begin{bmatrix} k_{\theta\theta} \end{bmatrix} \end{bmatrix}}^{k^{ij\tau s}} q_{i\tau} \tag{33}$$

The term $k_{\theta u}$ can be neglected when an external temperature is imposed as boundary condition, as in the present paper.

2. Results

The present model has been assessed considering the benchmark presented in [14]. A composite plate (see Figure 2) with dimensions: a=10 mm, b=4 mm, and h=1 mm has been considered. A four layers laminate with stacking sequence of $[0/90]_s$ has been used. The properties of the material are: $E_1 = 137.9$ GPa, $E_2 = E_3 = 14.48$ GPa, $G_{12} = G_{13} = G_{23} = 5.86$ GPa, $\nu_{12} = \nu_{13} = \nu_{23} = 0.21$ GPa, $\alpha_1 = 0.36\times 10^{-6}C^{-1}$ and $\alpha_2 = \alpha_3 = 28.8\times 10^{-6}C^{-1}$. The plate has a thermal load of 1 C. The transverse normal stress, σ_{zz} at the interface between the layers at 0 and 90 degree have been investigated. The through the thickness distribution of σ_{zz} at the free edge has been also considered. Equivalent single layer models, layer-wise models and mixed models have been compared.
Figure 3 shows the σ_{zz} distribution evaluated using equivalent single layer models with a different orders of expansion. The models are denoted as TE-n where n is the order, e.g. model TE4 is a fourth order model.
The results show that a first order model is not able to detect the normal through the thickness stress. An higher order model is required to detect the stress concentration. Figure 4 shows the through-the-thickness distribution of σ_{zz} at the free edge. The value of σ_{zz} is expected to be zero at the top and at the bottom of the plate but the present TE models are not able to fulfill the requirements.

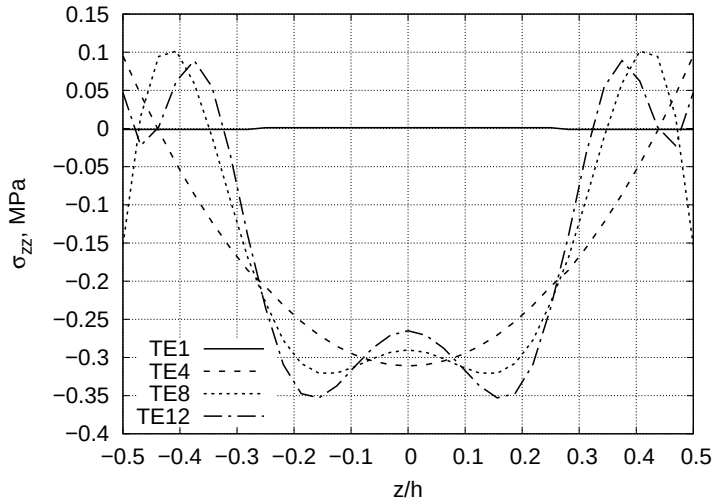

Figure 4 – Through-the-thickness distribution of σ_{zz} at the free edge evaluated using different ESL models.

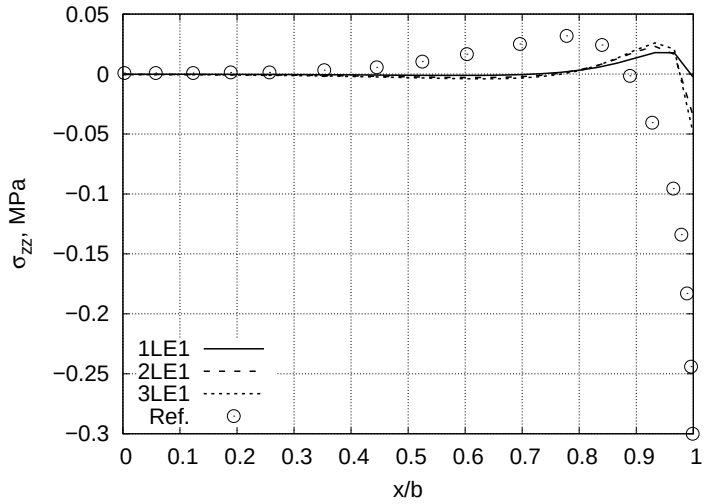

Figure 5 – σ_{zz} distribution evaluated using different Layer-wise linear models.

Figure 5 shows the σ_{zz} distribution, at the interface between the layer at 0 an 90 degree, evaluated using three different linear layer-wise approaches. The models are denoted using the nomenclature $k-LE-m$ where k is the number of elements for each layer and m is the order of the Lagrange expansion. Models 1LE1, 2LE1 and 3LE1 use one, two and three linear Lagrange elements on each layer.

Figures 6 and 7 show the σ_{zz} distributions using quadratic and cubic Lagrange expansion respectively. The results show that linear and quadratic elements are not able to detect the stress concentrations at the free edge. Cubic elements, see Figure 7, provide reliable results independently from the number of elements used through-the-thickness. Figure 8 shows that the use of at least two cubic elements for each layer leads to a fulfillment of the expected boundary condition with a value of σ_{zz} equal to zero at the top and at the bottom of the plate.

Figures 9 and 10 report the results for two models based on a NDK approach. Both models have a TE model up to x/b=0.7 and a LE models from x/b>0.7 . The use of a TE model in the central part of the plate lead to a reduction of the computational cost. The model 3LE3 has 53724 dof. The model 3LE3+TE4 uses a fourth order Taylor model in the central part and has 19164 dofs. Model 3LE3+TE8 has a eighth order TE mdoel in the central part and require 23484 dofs.

The results show that the use of the NDK approach can lead to accurate results with a significant reduction in the computational costs. The results provided by model 3LE3+TE4 are coparable with

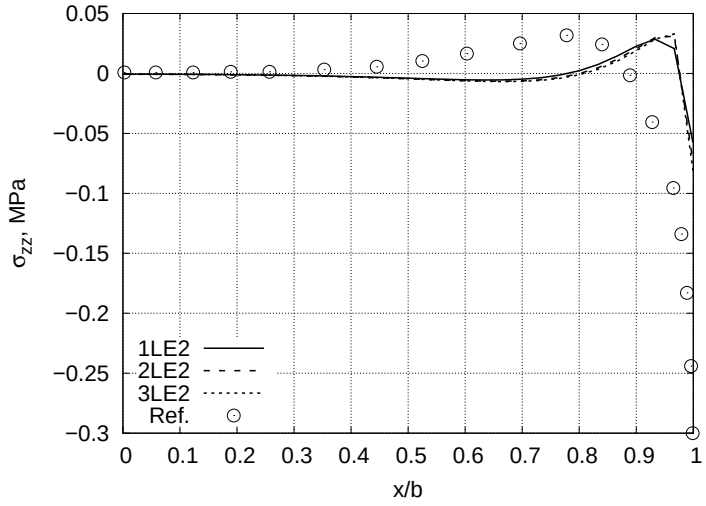

Figure 6 – σ_{zz} distribution evaluated using different Layer-wise quadratic models.

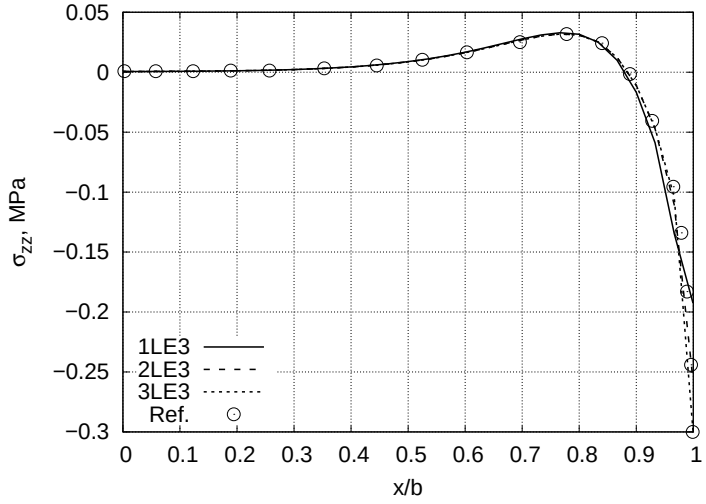

Figure 7 – σ_{zz} distribution evaluated using different Layer-wise cubic models.

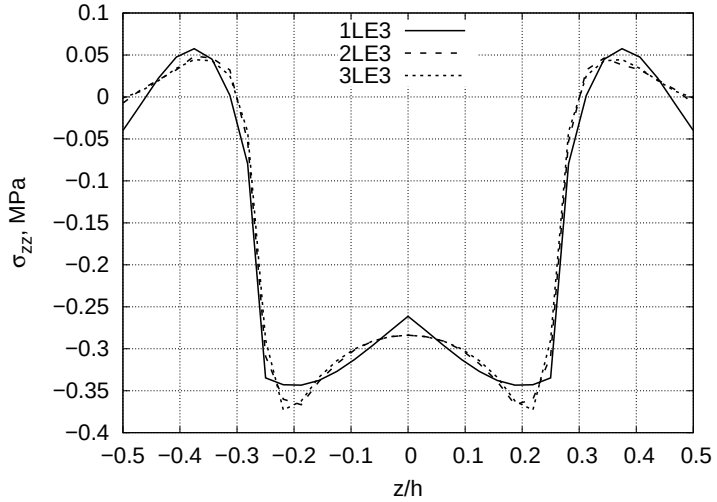

Figure 8 – Through-the-thickness distribution of σ_{zz} at the free edge evaluated using different cubic LE models.

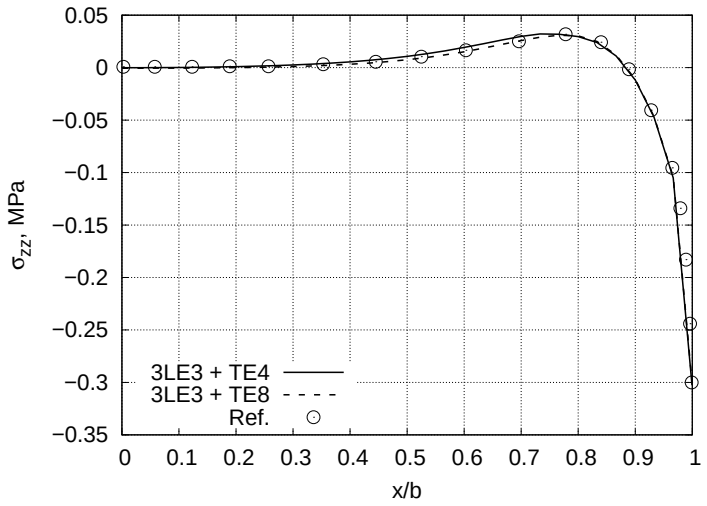

Figure 9 – σ_{zz} distribution evaluated using different NDK models.

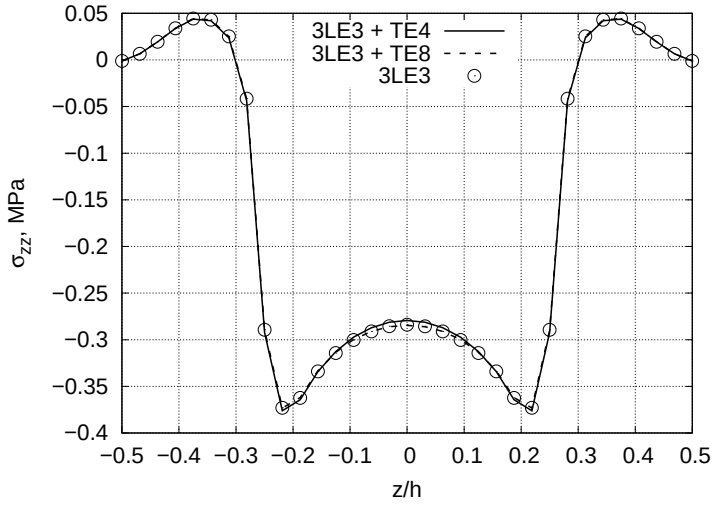

Figure 10 – Through-the-thickness distribution of σ_{zz} at the free edge evaluated using different NDK models.

those from model 3LE3 but with a reduction of the dofs of about 64%.

3. Conclusions

A refined kinematic model for the free-edge analysis of composite structures under thermal loads has been presented. The Carrera Unified Formulation has been used to derive the governing equations in a general form. Equivalent single layer model, as well as, layer-wise models have been adopted and compared. A node dependent kinematic model has been introduced to refine the results locally. The model has been assessed using the benchmark available in the open literature. From the results it is possible to state that:

- The use of refined kinematic models can lead to accurate results in the analysis of the free-edge stress of composite structures under thermal loads;
- The use of ESL models, up to a twelfth order, can lead to accurate results at the layers interface but is not able to fulfill the equilibrium condition at the top/bottom of the plate;
- A cubic layer-wise model is required to obtain an accurate stress field at the layers interfaces and through-the-thickness.
- A node dependent kinematic approach can be used to reduce the computational costs preserving the results accuracy.

4. Contact Author Email Address

mailto: enrico.zappino@polito.it

5. Copyright Statement

References

[1] Carrera, E., Brischetto, S., and Nali, P. Variational Statements and Computational Models for MultiField Problems and Multilayered Structures. *Mechanics of Advanced Materials and Structures 15*, 3-4 (2008), 182–198.

[2] Carrera, E., Cinefra, M., Li, G., and Kulikov, G. MITC9 shell finite elements with miscellaneous through-the-thickness functions for the analysis of laminated structures. *Composite Structures 154* (2016), 360–373.

[3] Carrera, E., Cinefra, M., Petrolo, M., and Zappino, E. *Finite element analysis of structures through Unified Formulation*. John Wiley & Sons, 2014.

[4] Carrera, E., Zappino, E., and Li, G. Analysis of beams with piezo-patches by node-dependent kinematic finite element method models. *Journal of Intelligent Material Systems and Structures 29*, 7 (2018), 1379–1393.

[5] Carrera, E., Zappino, E., and Li, G. Finite element models with node-dependent kinematics for the analysis of composite beam structures. *Composites Part B: Engineering 132* (jan 2018), 35–48.

[6] Dávila, C. G., Davila, C. G., and Dávila, C. G. Solid-to-shell transition elements for the computation of interlaminar stresses. *Computing Systems in Engineering 5*, 2 (apr 1994), 193–202.

[7] de Miguel, A. G., Pagani, A., and Carrera, E. Free-edge stress fields in generic laminated composites via higher-order kinematics. *Composites Part B: Engineering 168* (jul 2019), 375–386.

[8] He, J., and Zhang, Z. Bending analysis of antisymmetric angle-ply laminated plates including transverse shear effects. *Composite Structures 34*, 4 (1996), 437–444.

[9] Herakovich, C. T. On thermal edge effects in composite laminates. *International Journal of Mechanical Sciences 18*, 3 (1976), 129–134.

[10] Naghdi, P. The theory of plates and shells. *Handbuch der Physik, vol. VI a-2* (1972), 425–640.

[11] Pagano, N., and Hatfield, H. J. Elastic behavior of multilayered bidirectional composites. *AIAA Journal 10*, 7 (1972), 931–933.

[12] Reddy, J. N. A simple higher-order theory for laminated composite plates. *Journal of Applied Mechanics 51*, 4 (1984), 745–752.

[13] Srinivas, S., and Rao, A. A three-dimensional solution for plates and laminates. *Journal of the Franklin Institute 291*, 6 (1971), 469–481.

[14] Tahani, M., and Nosier, A. Free edge stress analysis of general cross-ply composite laminates under extension and thermal loading. *Composite Structures 60*, 1 (2003), 91–103.

[15] Zappino, E., Li, G., Pagani, A., and Carrera, E. Global-local analysis of laminated plates by node-dependent kinematic finite elements with variable ESL/LW capabilities. *Composite Structures 172* (jul 2017), 1–14.